

# COMPRESSED SENSING METAL ARTIFACT REMOVAL IN DENTAL CT

*Jiyoung Choi<sup>1</sup>, Min Woo Kim<sup>1</sup>, Won Seong<sup>2</sup>, and Jong Chul Ye<sup>1</sup>*

<sup>1</sup> Bio-Imaging & Signal Processing Lab., Dept. Bio& Brain Engineering  
Korea Advanced Institute of Science & Technology (KAIST)  
373-1 Guseong-dong Yuseong-gu, Daejeon 305-701, Korea  
<sup>2</sup>Chungnam National University  
79 Daehangno, Yuseong-gu, Daejeon 305-764, Korea

## ABSTRACT

Metal artifact removal (MAR) has been an important issue in dental X-ray CT due to the presence of metal implant and fillings. The practical use of most existing MAR methods have limitations due to their inherent drawbacks. In this research, we propose a novel MAR algorithm in dental CT. Based on the sparse volume occupation of the metallic inserts, we can formulate the MAR problem as a sparse recovery problem within the compressed sensing framework. One of the main advantages of employing compressed sensing theory in MAR problem is that the sparseness of the metallic objects allows us to reduce the view samples significantly without loss of image quality, accelerating the proposed MAR algorithm drastically. Experimental results using real dental CT scanner measurements show that our algorithm can perform accurate metallic artifact removal very quickly.

**Index Terms**— Metal artifact removal, compressed sensing, dental X-ray CT, sparsity

## 1. INTRODUCTION

For the circular source trajectory, an approximated inversion algorithm called Feldkamp, Davis and Kress (FDK) algorithm is most widely used. Even though FDK algorithm introduces the cone beam artifacts, the amount of cone beam artifacts in dental applications is minimal since the region of interests is the area around the jaw which is usually placed at the mid-plane of circular trajectory. Rather, more serious problems in dental CT come from the usual placements of metallic implant and dental fillings, which cause severe metal artifacts. In presence of metallic inserts, x-ray photons cannot penetrate the metallic object consistently due to beam hardening, poor signal to noise ratio (SNR), nonlinear partial volume effect (NLPV), scatter, noise and etc. The inconsistency of projections introduce severe streaking and shading artifacts in the reconstructed images using FDK algorithm.

Linear interpolation (LI) is one of the most traditional and simplest ways for metal artifact removal (MAR). However, it loses entire information about metallic implants by replacing the sinogram corresponding to metallic parts with only linear interpolated values from the boundaries. Although other interpolation method using wavelets has proposed to supplement this loss of information, the general application have difficulties due to heuristic determination of parameters. Iterative reconstruction methods, such maximum-likelihood (ML) and iterative maximum-likelihood polychromatic algorithm for CT (IMPACT) [1], is another method for MAR. Even though the reconstruction results from iterative reconstruction often exhibit nearly free of metallic artifacts, the main drawbacks include its extremely high computational complexity and requirements for accurate modelling of the physical measurement process.

This paper is mainly interested in developing a novel MAR algorithm that can be applied even for geometries with truncated projection and width truncated detector. Our main concern is the removal of artifact caused by the metallic insertions located within FOV with sparse support. By separately reconstruct the background and metallic parts, the conditions are easily satisfied in most of dental CT cases since the jaw structure with metallic inserts should be included within FOV to accommodate the diagnosis.

The sparsity of metallic inserts allow us to use the compressed sensing (CS) theory that has been recently emerged as a major research thrust among signal processing community [2]. Even though the original metal artifact removal problem in dental CT is not measurement limited due to the sufficient measurements during acquisition, the compressed sensing still provides us great advantages from practical aspects. More specifically, by exploiting the sparseness of metallic objects, CS guarantees the accurate reconstruction even from aggressive angular down-sampling, which significantly reduces the total computational burden of iterative process even without using any hardware acceleration. Furthermore, even without accurate calibration of model parameters as required in the conventional iterative MAR, compressed sensing algo-

---

This work has been supported by the funding of Vatech & E-Woo Co.

rithm imposes the consistency of the sinogram data based on sparsity of metallic objects, which makes the algorithm very powerful in many complicated scanner geometries including projection truncation.

## 2. PROJECTION TRUNCATION DENTAL CT GEOMETRY

In this section, we introduce a projection truncation CT geometry, which is our main hardware platform for MAR experiments. Consider a circular cone-beam CT geometry in Figure 1, where only the gray area of the detector plane corresponds to the active detector elements. Compared to conventional circular geometry, this geometry allows smaller size detector, which lowers the overall system cost. However, this introduces two types of projection truncation originated from 1) asymmetric placement of detector along the center, and 2) the fact that the skull is not entirely included within FOV.

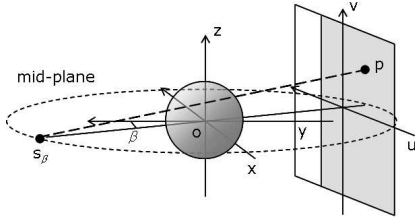


**Fig. 1.** Schematic representation of width truncated cone beam CT geometry with reduced size of detectors. Gray part corresponds to the active detector area.

To deal with the first type of projection truncation, Cho et al. [3] demonstrated that faithful reconstruction can be obtained within FOV by applying the optimal weighting along the horizontal direction of sinogram measurement. With the weighting function  $\lambda(u)$ , the modified sinogram can be defined as  $\hat{p}_\beta(u, v) = \lambda(u)p_\beta(u, v)$  where  $p_\beta(u, v)$  denotes the projection for the gantry rotation angle  $\beta$ . Then, the estimated linear attenuation coefficient  $\hat{\mu}(x, y, z)$  using the FDK algorithm is given by

$$\hat{\mu}(x, y, z) = \frac{1}{2} \int_0^{2\pi} \left( \frac{D}{R - y_\beta} \right)^2 \times \int_{-\infty}^{\infty} \hat{p}_\beta(u, v) h \left( \frac{Dx_\beta}{R - y_\beta} - u \right) \frac{D}{\sqrt{D^2 + u^2 + v^2}} du d\beta. \quad (1)$$

where  $h(u)$  denotes a ramp filter along horizontal axis of detector domain, and  $D$  and  $R$  refer the distance from source to detector and origin, respectively. The vertical coordinates  $z$  and  $v$  are related as  $v = \frac{Dz}{R - y_\beta}$ . The image coordinates with rotated angle  $\beta$  are referred as  $x_\beta$  and  $y_\beta$ .

One assumption of FDK reconstruction is that x-ray is monochromatic. However, most of the real x-ray source is

polychromatic given as follows :

$$\hat{m}_i = \sum_{k=1}^K b_{ik} \exp \left( - \sum_{j=1}^N l_{ij} \mu_{jk} \right) \quad (2)$$

where  $\mu_{jk} = \mu_j(E_k)$  is the linear attenuation coefficients in pixel  $j$  at energy level  $k$ , and  $l_{ij}$  is the effective intersection length of projection line  $i$  with voxel  $j$ . The total energy that would be detected in the absence of absorber is denoted  $b_{ik}$ . The discrepancy between the assumption and the measurement Eq. (2) introduces the inconsistency in sinogram, which is the main source of the metallic artifacts.

One of the most complete metal artifact removal algorithms that consider the polychromatic x-ray spectrum is so-called iterative maximum-likelihood (ML) polychromatic algorithm for CT (IMPACT) [1]. IMPACT assume that x-ray photon follows the Poisson distribution with mean and variance of  $\{\hat{m}_i\}_{i=1}^M$ . Under the independent noise assumption, the log-likelihood of probability density function for the measurement vector is given by

$$L(\mathbf{m}) = \sum_{i=1}^M (m_i \ln(\hat{m}_i) - \hat{m}_i). \quad (3)$$

The IMPACT then incorporates the general acquisition model Eq. (2) into Eq. (3). IMPACT estimates the effective intersection length  $l_{ij}$  from the transmission measurement  $\{m_i\}_{i=1}^M$  by iteratively maximizing the loglikelihood Eq. (3). Even though IMPACT can significantly remove the metal artifact by precise modeling, it cannot be applied to our projection truncation dental CT due to the projection truncation, and the extremely large number of voxels and projection data for dental CT applications.

## 3. COMPRESSED SENSING MAR

Unlike the conventional compressed sensing applications, the whole jaw structure is not necessarily sparse in some basis in our metal artifact removal algorithm. Rather, our algorithm assumes that the non-metallic background can be reconstructed separately, making the residual image sparse.

More specifically, we first define the sinogram  $\hat{p}_i$  and its noisy measurement  $p_i$ :

$$\hat{p}_i = -\ln \frac{\hat{m}_i}{b_0} = \sum_{j=1}^N l_{ij} \mu_j, \quad p_i = -\ln \frac{m_i}{b_0}. \quad (4)$$

After decompose the unknown linear attenuation coefficients  $\{\mu_i\}_{i=1}^N$  into background reconstruction  $\{\mu_i^C\}_{i=1}^N$ , using LI method, and the residual images  $\{\Delta\mu_i\}_{i=1}^N$ , which are mainly composed of metallic parts, the following quantities are introduced:

$$\Delta p_i = -\ln \frac{m_i}{b_0} - \hat{p}_i^C, \quad \Delta \hat{p}_i = \sum_{j=1}^N l_{ij} \Delta \mu_j, \quad i = 1, \dots, M. \quad (5)$$

Then, applying Taylor series approximation about  $\Delta p_i$ , the log-likelihood Eq. (3) can be approximated as a weighted  $l_2$  norm cost function:

$$L(\Delta\boldsymbol{\mu}) \approx -\frac{1}{2} \|\Delta\mathbf{p} - \mathbf{L}\Delta\boldsymbol{\mu}\|_{\mathbf{M}}^2 + \text{const.}$$

where  $\Delta\mathbf{p} = \{\Delta p_i\}_{i=1}^M \in \mathbb{R}^M$ ,  $\Delta\boldsymbol{\mu} = \{\Delta\mu_i\}_{i=1}^N \in \mathbb{R}^N$  and  $\mathbf{L} = [l_{ij}] \in \mathbb{R}^{M \times N}$ , and  $\mathbf{M}$  denotes the diagonal matrix  $\mathbf{M} = \text{diag}(m_i)$ , respectively. Therefore, the resultant  $l_1$  minimization problem for metal artifact removal under Poisson noise model is given by imposing the sparsity of  $\Delta\boldsymbol{\mu}$ :

$$\begin{aligned} & \text{minimize} && \|\Delta\boldsymbol{\mu}\|_1 \\ & \text{subject to} && \|\Delta\mathbf{p} - \mathbf{L}\Delta\boldsymbol{\mu}\|_{\mathbf{M}}^2 < \epsilon \end{aligned} \quad (6)$$

Note that not like typical compressed sensing applications, Eq. (6) is *not* underdetermined. However, we *purposefully* convert the overdetermined  $l_1$  minimization problem in Eq. (6) to an underdetermined problem mainly due to the *computational* reason. Since the metallic parts only assume very sparse supports from FOV, the minimum angular view numbers for accurate reconstruction of metallic parts should be order of magnitude smaller than that required for FDK. Therefore, the final optimization problem we want to address is

$$\begin{aligned} & \text{minimize} && \|\Delta\boldsymbol{\mu}\|_1 \\ & \text{subject to} && \|\Delta\mathbf{p}^P - \mathbf{L}^P\Delta\boldsymbol{\mu}\|_{\mathbf{M}}^2 < \epsilon, \quad P \ll M \end{aligned} \quad (7)$$

where  $\Delta\mathbf{p}^P \in \mathbb{R}^P$  is angularly downsampled sinogram data from  $\Delta\mathbf{p} \in \mathbb{R}^M$ , and  $\mathbf{L}^P \in \mathbb{R}^{P \times N}$  denotes the corresponding submatrix composed of the effective intersection lengths of projection lines corresponding to  $\Delta\mathbf{p}^P$ , respectively.

In addition to the computational acceleration, our compressed sensing MAR algorithm Eq. (7) has another important advantage. As described before, the whole objects are not always included within a FOV due to the limited detector size, as shown in Figure 2. However, the metallic parts are usually contained within FOV, iterative optimization methods can be applied without any problem.

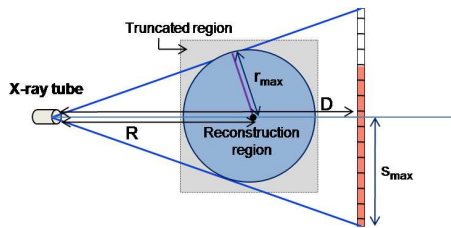


**Fig. 2.** The lightly colored part in image is truncated since all the part of image cannot be included to all projections. Colored detector shows real detector region in width-truncated CT.

The standard method to solve  $l_1$  minimization problem, so-called basis pursuit, is computationally very expensive

especially for dealing with large data set such as image or volume data. Hence, in this paper, we employ an iterative reweighted  $l_2$ -norm method called FOCal Underdetermined System Solver (FOCUSS) [4] to address the optimization problem Eq. (6).

## 4. EXPERIMENTAL RESULTS

For physical experiments, the projection data was measured using a clinical dental CT system (Picasso Trio, EWO, Korea) that has width-truncated geometry as shown in Figure 1.

### 4.1. Phantom Experiment Results

A physical phantom had been constructed with 10 metal nails fixed in a plate slightly tilted.

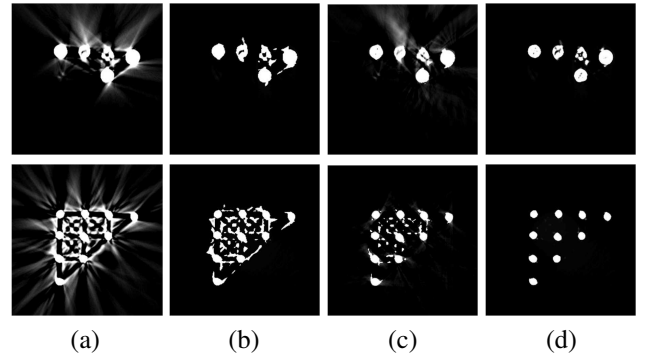


**Fig. 3.** Two different axial sections of reconstructed phantom are shown at top and bottom. Images are reconstructed by (a) FDK, (b) LI with a lower threshold (0.08), (c) LI with a higher threshold (0.12), and (d) CS-MAR using a threshold (0.08).

The WBP reconstruction in Figure 3(a) has severe streaking artifact especially between the metallic nails. The artifacts are not completely removed by LI as shown in Figure 3(b) and (c), whose thresholds values for metallic parts are differently set.<sup>1</sup> From the LI results in Figure 3(b) and (c), we have observed interesting trade-off between threshold and artifact removal in the LI approach. Although metallic insertion can be more clearly segmented with higher threshold, more severe metallic artifact still remains in background reconstruction. This is one of the fundamental limits of the LI approach.

However, CS-MAR is relatively free of such threshold dependent trade-off, since such spurious segmented noises can be effectively removed during FOCUSS update. Those spurious segmented parts from the low threshold value as used in Figure 3(b) can be effectively removed after six iterations of CS-MAR, as shown in Figure 3(d). Furthermore, even the inner structure of nails is visible in CS-MAR result. For the CS-MAR only 25 acquired views are used for reconstruction.

<sup>1</sup>Note that this number is a not a Hounsfield unit (HU) due to the specific scanner vendor's proprietary specs.

## 4.2. In Vivo Results

Since various types of metal insertions can be located in one patient's jaw in *in vivo* experiment, the threshold values for LI and CS-MAR were chosen in between the lowest intensity of metal insertion and anatomic structures.

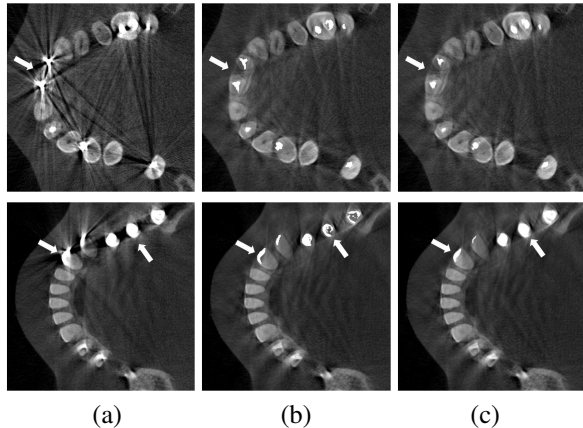


**Fig. 4.** The axial sections of reconstruction from two different *in vivo* samples are shown in top and bottom, respectively. Each image is reconstructed using (a) FDK, (b) LI, and (c) CS-MAR. For better comparison, images are magnified in jaw area. All the slices are shown at the same gray scale.

In both of LI and CS-MAR, the streaking and shading artifacts laid in WBP are mostly gone so that we can verify the dental structure in arrowed region. Even though the background artifacts are removed, in LI result the metallic insertions have spurious shape since the metallic artifacts were included during the segmentation. On the other hand, CS-MAR can reconstruct dental filling more realistically by removing the spurious artifacts. The CS-MAR results, shown in top (bottom) row, were obtained using only 23 (25) views (corresponding to 1/20 (1/30) downsampling factor compare to WBP result, using 455 (727) views) and after three FOCUSS iterations. Considering the size of volume data and the projection data, we can easily see the huge computational advantages of our CS-MAR over the fully iterative methods.

Even though most of MAR methods have been evaluated based on the reconstruction quality of axial sections, in diagnosis of teethridge infection, sagittal and coronal sections are, however, important as much as axial sections. Especially, the dark shadow between metallic inserts are often misdiagnosed as inflammation. So the removal of such artifacts are one of the most important criteria from a clinical perspective. In Figure 5, we can confirm that CS-MAR outperforms conventional MAR method for the sagittal and coronal sections, as well as axial sections.

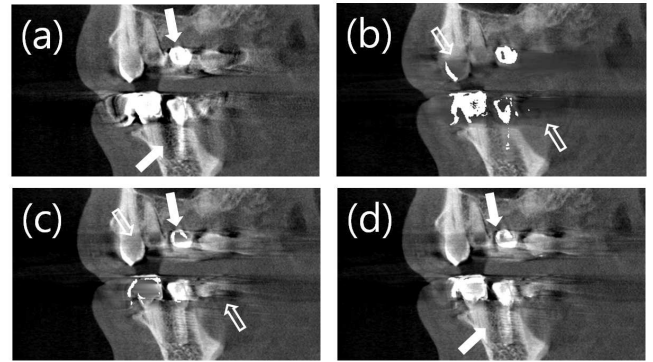


**Fig. 5.** A sagittal slice of reconstruction using (a) FDK, (b) LI(0.08), (c) LI(0.14), and (d) CS-MAR(0.14). The filled arrows show the remarkable difference between algorithms, whereas unfilled arrows compare LI results with different thresholds.

## 5. CONCLUSION

Since the metallic objects usually occupy sparse support within a FOV, we can apply compressed sensing approach to MAR problem. The obtained  $l_1$  penalized maximum likelihood criterion was implemented by a reweighted norm approach using FOCUSS. In phantom and *in vivo* experiments, the proposed CS-MAR outperformed FDK and LI in both restoring the original shape of the metallic inserts as well as removing the shadow artifact that could lead to misdiagnosis. Furthermore, compressed sensing theory allows aggressive view downsampling, which results in significant reduction of the overall computational time of CS-MAR.

## 6. REFERENCES

- [1] B. De Man, J. Nuyts, P. Dupont, G. Marchal, and P. Suetens, "An iterative maximum-likelihood polychromatic algorithm for CT," *IEEE Trans. on Medical Imaging*, vol. 20, no. 10, pp. 999–1008, 2001.
- [2] D. L. Donoho, "Compressed sensing," *IEEE Trans. on Information Theory*, vol. 52, no. 4, pp. 1289–1306, April 2006.
- [3] Paul S. Cho, Anthony D. Rudd, and Roger H. Johnson, "Cone-beam CT from width-truncated projection," *Computerized Medical Imaging and Graphics*, vol. 20, no. 1, pp. 49–57, 1996.
- [4] I. F. Gorodnitsky, J. S. George, and B. D. Rao, "Neuromagnetic source imaging with FOCUSS: a recursive weighted minimum norm algorithm," *Electroencephalogr Clin Neurophysiol.*, vol. 95, no. 4, pp. 231–51, October 1995.